ORIGINAL PAPER

Pentose degradation in archaea: *Halorhabdus* species degrade D-xylose, L-arabinose and D-ribose via bacterial-type pathways

Jan-Moritz Sutter[1] · Ulrike Johnsen[1] · Andreas Reinhardt[1] · Peter Schönheit[1]

Abstract

The degradation of the pentoses D-xylose, L-arabinose and D-ribose in the domain of archaea, in *Haloferax volcanii* and in *Haloarcula* and *Sulfolobus* species, has been shown to proceed via oxidative pathways to generate α-ketoglutarate. Here, we report that the haloarchaeal *Halorhabdus* species utilize the bacterial-type non-oxidative degradation pathways for pentoses generating xylulose-5-phosphate. The genes of these pathways are each clustered and were constitutively expressed. Selected enzymes involved in D-xylose degradation, xylose isomerase and xylulokinase, and those involved in L-arabinose degradation, arabinose isomerase and ribulokinase, were characterized. Further, D-ribose degradation in *Halorhabdus* species involves ribokinase, ribose-5-phosphate isomerase and D-ribulose-5-phosphate-3-epimerase. Ribokinase of *Halorhabdus tiamatea* and ribose-5-phosphate isomerase of *Halorhabdus utahensis* were characterized. This is the first report of pentose degradation via the bacterial-type pathways in archaea, in *Halorhabdus* species that likely acquired these pathways from bacteria. The utilization of bacterial-type pathways of pentose degradation rather than the archaeal oxidative pathways generating α-ketoglutarate might be explained by an incomplete gluconeogenesis in *Halorhabdus* species preventing the utilization of α-ketoglutarate in the anabolism.

Keywords *Halorhabdus utahensis* · D-ribose · D-xylose and L-arabinose · Archaea · Xylose isomerase · Ribokinase · Lateral gene transfer

Introduction

The pentoses D-xylose, L-arabinose and D-ribose are abundant in nature being part of hemicellulose material of plants and as component of ribonucleotides. Thus, these pentoses are common growth substrates of many microorganisms. The pathways of pentose degradation have been well studied in bacteria and fungi. In most bacteria D-xylose, L-arabinose and D-ribose are non-oxidatively degraded to xylulose-5-phosphate, an intermediate of the pentose phosphate

✉ Peter Schönheit
peter.schoenheit@ifam.uni-kiel.de

1 Institut für Allgemeine Mikrobiologie, Christian-Albrechts-Universität Kiel, Am Botanischen Garten 1-9, 24118 Kiel, Germany

pathway, involving specific sugar kinases, isomerases and epimerases (Fig. 1a). The degradation of D-xylose involves xylose isomerase and xylulokinase, and of L-arabinose the enzymes arabinose isomerase, ribulokinase and L-ribulose-5-phosphate-4-epimerase. Further, D-ribose conversion to xylulose-5-phosphate is catalyzed by ribokinase, ribose-5-phosphate isomerase and D-ribulose-5-phosphate-3-epimerase (van de Werken et al. 2008).

In the domain of archaea, the degradation of D-xylose, L- and D-arabinose were studied in detail in the haloarchaea *Haloferax volcanii*, the *Haloarcula* species *H. marismortui* and *H. hispanica*, and in the thermoacidophilic *Sulfolobus* species *S. solfataricus* and *S. acidocaldarius*. In *H. volcanii* D-xylose and L-arabinose are degraded to α-ketoglutarate via an oxidative pathway involving specific dehydrogenases for D-xylose and L-arabinose oxidation and promiscuous pentonolactonase and pentanonate dehydratase. Further, α-ketoglutarate is formed by a 2-keto-3-deoxypentanonate dehydratase and an α-ketoglutarate semialdehyde dehydrogenase (Johnsen et al. 2009, 2013; Sutter et al. 2017). The degradation of D-ribose in archaea has been elucidated
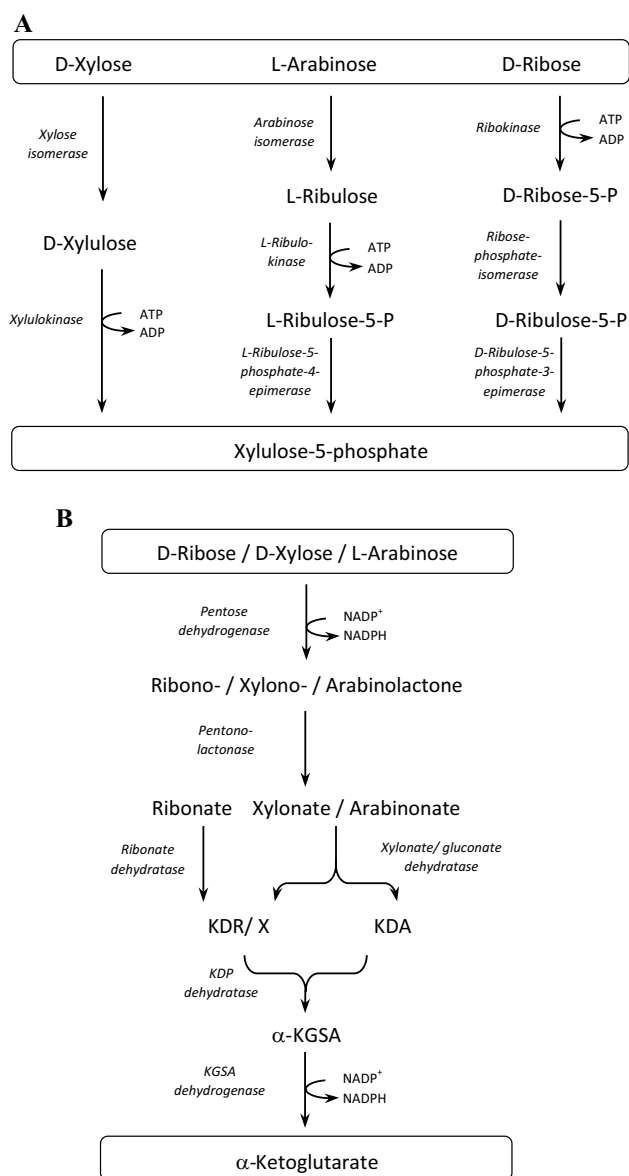
Fig. 1 Proposed pathways of pentose degradation in bacteria and archaea. **a** Non-oxidative degradation pathways of D-xylose, L-arabinose and D-ribose to xylulose-5-phosphate operative in most bacteria. **b** Oxidative degradation pathway of D-ribose, D-xylose and L-arabinose to α-ketoglutarate in the *Haloarcula* species *H. maris-mortui* and *H. hispanica*. Abbreviations: KDR, 2-keto-3-deoxyribonate; KDX, 2-keto-3-deoxyxylonate; KDA, 2-keto-3-deoxyarabinonate; α-KGSA, α-ketoglutarate semialdehyde; KDP dehydratase, 2-keto-3-deoxypentanonate dehydratase

in *Haloarcula* species, which unlike *H. volcanii* utilize D-ribose. It was found that *Haloarcula* species evolved a novel oxidative pathway of pentose degradation that allows the degradation of D-ribose, in addition to D-xylose and L-arabinose (Johnsen and Schönheit 2004; Johnsen et al. 2020). This degradation pathway involves novel promiscuous enzymes, pentose dehydrogenase and pentonolactonase,

that show an expanded substrate specificity for D-ribose and ribonolactone, respectively (Fig. 1b). Further, a novel highly specific dehydratase for ribonate has been identified forming a novel family within the enolase superfamily. The final conversion of 2-keto-3-deoxyribonate to α-ketoglutarate proceeds via 2-keto-3-deoxypentanonate dehydratase and α-ketoglutarate semialdehyde dehydrogenase that are homologous to the respective *H. volcanii* enzymes. In *Sulfolobus* species D-xylose, L- and D-arabinose are oxidatively degraded to α-ketoglutarate and/or malate (Brouns et al. 2006; Nunn et al. 2010; Wagner et al. 2018).

Based on bioinformatic analyses of ten haloarchaeal genomes (Anderson et al. 2011) it has been reported that *Halorhabdus utahensis*—unlike other haloarchaea—contains classical bacterial-like genes of D-xylose and L-arabinose degradation to xylulose-5-phosphate. So far, transcriptional analyses of these genes during growth on pentoses and the catalytic properties of the encoded enzymes have not been analyzed.

Here, we report transcription of selected genes of D-xylose and L-arabinose degradation in *H. utahensis* and the characterization of their encoded enzymes. Further, we found that D-ribose is degraded in *H. utahensis* and *Halorhabdus tiamatea* to xylulose-5-phosphate by the bacterial pathway involving the enzymes ribokinase, ribose-5-phosphate isomerase and D-ribulose-5-phosphate-3-epimerase. Together, the data indicate that in *Halorhabdus* species pentoses are degraded by the classical—non-oxidative—degradation pathways found in most bacteria. Thus, the genus *Halorhabdus* differs from other closely related haloarchaea that degrade pentoses via oxidative pathways. It is proposed that *Halorhabdus* species acquired their pentose catabolic pathways from bacteria via lateral gene transfer.

Materials and methods

Growth of *Halorhabdus utahensis*

Halorhabdus utahensis (DSM12940) was grown under aerobic conditions at 37 °C on a modified version of the DSMZ medium number 927; the Tris-buffer was exchanged by 3-morpholinopropane-1-sulfonic acid buffer (0.1 M). D-Xylose, D-ribose, L-arabinose or D-glucose (each 15 mM) were used as carbon and energy sources. Growth was followed by measuring the optical density at 600 nm; during growth, samples were taken for measuring the substrate consumption using the Orcinol assay (Johnsen and Schönheit 2004).

Purification of ribokinase activity from D-ribose grown *H. utahensis*

Cell extract was prepared in 100 mM Tris–HCl (pH 8.0) containing 2 M ammonium sulfate. After application on a Phenyl-Sepharose column, protein was eluted by decreasing the concentration of ammonium sulfate. Fractions containing ribokinase activity (measured with 20 mM D-ribose and 2.5 mM ATP) were further purified by size exclusion chromatography using a Superdex 200 column and 50 mM Tris–HCl (pH 7.5) containing 2 M potassium chloride. Fractions showing ribokinase activity were applied on a Q-Sepharose column in 50 mM Tris–HCl (pH 8.8) containing 0.15 M NaCl and 50 mM MgCl$_2$. Protein was eluted by increasing the concentration of NaCl up to 1 M. At this stage, the protein was partially pure as analyzed by SDS-PAGE, and was used for MALDI-TOF analysis.

Overexpression and purification of recombinant enzymes

Genes were amplified from genomic DNA of *H. utahensis* and each PCR product was cloned into pTA963 using the cloning strategy as described (Allers et al. 2010) (Supplemental Table S1). *H. volcanii* H1209 was transformed with the respective plasmids and expression of each gene was performed in complex medium at 42 °C (Allers et al. 2010); expression was induced by the addition of 2 mM tryptophan. After 18 h of further growth, cells were harvested by centrifugation. Cell pellets were suspended in 50 mM Tris–HCl (pH 8.2) containing 1.5 M KCl, 50 mM MgCl$_2$ and 5 mM imidazole and disruption was performed by passing the cells through a French pressure cell followed by a centrifugation step. The supernatants were applied onto a nickel–nitrilotriacetic acid (Ni–NTA) column and specific elution of proteins was performed with 100 mM imidazole. Further purification was performed by size-exclusion chromatography on a Superdex HiLoad 200 column in 50 mM Tris–HCl (pH 7.5) containing 1.5 or 2 M KCl. At this stage most of the proteins were essentially pure. Xylulokinase was further purified on a Phenyl-Sepharose column equilibrated in 50 mM Tris–HCl (pH 8.0) containing 2 M ammonium sulfate. Elution of the protein was performed by decreasing the concentration of ammonium sulfate.

Determination of native molecular masses of recombinant enzymes

Size-exclusion chromatography was performed with a flow rate of 1 ml/min using a Superdex 200 HiLoad column (1.6 by 60 cm) (GE Healthcare, Freiburg, Germany). For calibration of the column, the HMW and LMW kits (GE Healthcare) were used. For the calculation of the oligomeric structures of the enzymes, the calculated molecular masses of subunits were used. The subunit sizes measured with SDS-PAGEs were higher than the calculated masses due to the acidic nature of extremely halophilic proteins (Pickl et al. 2014).

Characterization of recombinant enzymes

Xylose isomerase was measured at 37 °C in 0.1 M Tris–HCl (pH 8.0) containing 2 M KCl, 20 mM MgCl$_2$, 1 mM CoCl$_2$ and 100 mM D-xylose. D-Glucose and L-arabinose were tested as alternative substrates. During incubation (0–30 min), aliquots were taken and the reaction was stopped by the addition of trichloroacetic acid to a final concentration of 10%. After centrifugation product formation was quantified by the cysteine-carbazole method (Horecker 1988).

Xylulokinase was measured at 37 °C in 0.1 M Tris–HCl (pH 8.0) containing 2 M KCl, 10 mM MgCl$_2$, 0.3 mM NADH, 1 mM phosphoenolpyruvate, 12.5 mM ATP, 10 mM D-xylulose, 6 U pyruvate kinase and 9 U lactate dehydrogenase.

Arabinose isomerase was measured at 37 °C in 0.1 M Tris–HCl (pH 8.0) containing 2 M KCl, 20 mM MgCl$_2$, 1 mM CoCl$_2$ and 50 mM L-arabinose. During incubation (0–20 min) aliquots were taken and L-ribulose was quantified by the cysteine-carbazole method.

Ribulokinase was measured at 37 °C in 0.1 M Tris–HCl (pH 8.0) containing 1.5 M KCl, 50 mM MgCl$_2$, 0.3 mM NADH, 1 mM phosphoenolpyruvate, 10 mM ATP, 1 mM L-ribulose, 6 units pyruvate kinase and 9 units lactate dehydrogenase.

Ribokinase was measured at 42 °C in 0.1 M bis–tris (pH 7.5) containing 1.5 M KCl, 0.3 mM NADH, 2.5 mM phosphoenolpyruvate, 10 mM MgCl$_2$, 5 mM ATP, 5 mM D-ribose, 1 U pyruvate kinase and 5 U lactate dehydrogenase.

Ribose-5-phosphate isomerase was measured at 37 °C in 0.1 M Tris–HCl (pH 8.0) containing 2 M KCl, 20 mM MgCl$_2$ and 80 mM D-ribose-5-phosphate. Alternative substrates were tested at 10 mM and 100 mM. During incubation (0–10 min), aliquots were taken and activity was detected by the cysteine-carbazole method.

Enzyme activities of the oxidative pentose degradation pathways, i.e., xylose dehydrogenase, arabinose dehydrogenase, ribonate dehydratase and α-ketoglutarate dehydrogenase, were measured in cell extracts according (Johnsen et al. 2009, 2020, 2013).

Transcriptional analyses

RNA was prepared from exponentially grown cells of *H. utahensis* (optical density at 600 nm of about 0.5) as described (Johnsen et al. 2013). Northern blot analyses were

performed with 2 to 8 µg RNA (Pickl et al. 2012). Probes were generated by PCR using the PCR digoxigenin (DIG) probe synthesis kit (Roche Diagnostics, Mannheim, Germany) (primers are summarized in Supplemental Table S1). Sizes of transcripts were calculated with the RiboRuler high-range RNA ladder (Thermo Fisher Scientific, Schwerte, Germany).

Sequence and phylogenetic analyses

BlastP analyses were performed using the RefSeq database at NCBI (O'Leary et al. 2016). Sequence alignments were generated with ClustalX 2.1 using default parameters and are provided with ESPRIPT (Larkin et al. 2007; Robert and Gouet 2014). Secondary structure elements of xylose isomerase and ribokinase of *Halorhabdus* species were predicted using the PSIPRED server (Buchan et al. 2013). Phylogenetic trees are based upon a multiple-amino-acid sequence alignment that was generated with ClustalX (Larkin et al. 2007). Numbers at the nodes are bootstrapping values according to neighbor joining (NJ).

Results and discussion

Genome analyses indicate that *Halorhabdus utahensis* unlike other haloarchaea contains genes encoding putative enzymes of the classical pathways of D-xylose and L-arabinose degradation reported for most bacteria (Anderson et al. 2011). We performed transcript analyses of selected genes of the bacterial pathways and analyzed the molecular and catalytic properties of the encoded enzymes. Also, D-ribose degradation in *H. utahensis* and *Halorhabdus tiamatea* and the enzymes involved were studied revealing the operation of the bacterial-type pathway of D-ribose degradation.

D-xylose degradation to xylulose-5-phosphate in *H. utahensis*

H. utahensis grew on D-xylose with a doubling time of 17 h up to optical densities at 600 nm of about 1.0 (Fig. 2a). Genome analysis of *H. utahensis* revealed the absence of genes encoding key enzymes of the oxidative xylose degradation to α-ketoglutarate, i.e., 2-keto-3-deoxyxylonate dehydratase and α-ketoglutarate semialdehyde dehydrogenase found in other haloarchaeal species. In addition, extracts of D-xylose-grown *H. utahensis* cells do not contain activity of α-ketoglutarate semialdehyde dehydrogenase and also of xylose dehydrogenase, the first enzyme of the oxidative degradation pathway. Instead, extracts of D-xylose-grown *H. utahensis* cells contain activities of xylose isomerase (0.049 U/mg) and xylulokinase (0.408 U/mg) and the genes
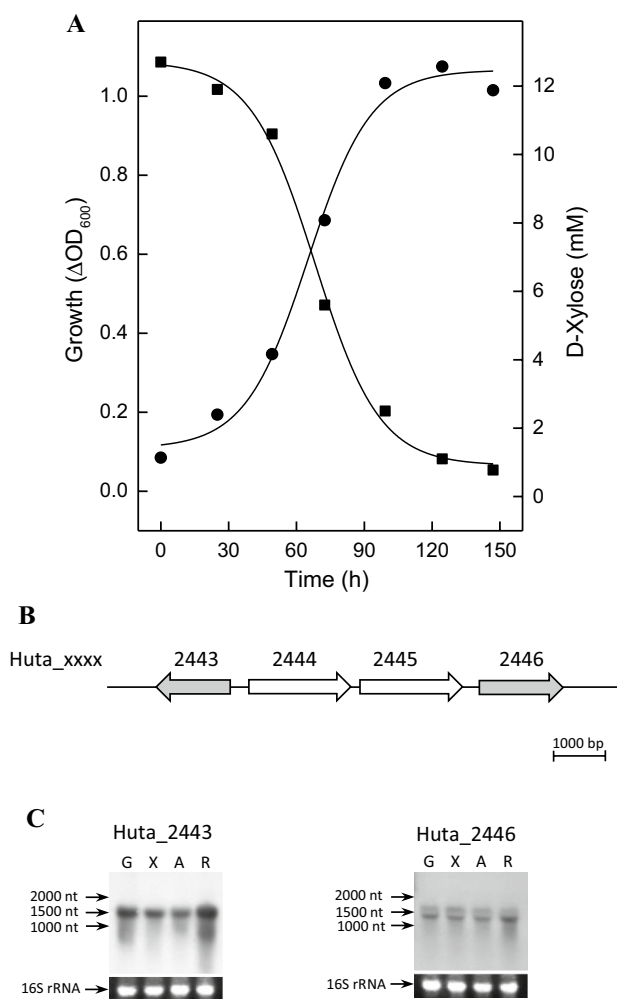
Fig. 2 Xylose degradation in *Halorhabdus utahensis*. **a** Growth was performed at 37 °C on 15 mM D-xylose in synthetic medium (filled circle); consumption of D-xylose (filled square). **b** Genome organization of Huta_2443 and Huta_2446 encoding putative xylose isomerase and xylulokinase, respectively (arrows in grey); the genes Huta_2444 and Huta_2445 encode putative methyl-accepting chemotaxis proteins (arrows in white). **c** Northern blotting of Huta_2443 and Huta_2446 was performed with RNA from cells grown on D-glucose (G), D-xylose (X), L-arabinose (A) and D-ribose (R). 16S rRNA served as loading control

Huta_2443 and Huta_2446 were identified that encode putative xylose isomerase and xylulokinase (Fig. 2b).

Transcription of Huta_2443 and Huta_2446 was followed by Northern blot analyses using RNA from cells grown on D-xylose, L-arabinose, D-ribose and D-glucose. As indicated in Fig. 2c a strong transcriptional signal at 1500 nucleotides was detected for both genes in cells grown on the three pentoses as well as on D-glucose; the transcript sizes correspond to that of Huta_2443 (1317 nucleotides) and of Huta_2446 (1548 nucleotides). The presence of transcripts in both D-glucose- and pentose-grown cells indicates that the genes are constitutively expressed. It should be noted that

the genes of D-xylose degradation in bacteria are specifically regulated by D-xylose (Luo et al. 2014).

Huta_2443 and Huta_2446 were overexpressed in *Haloferax volcanii* H1209 and the recombinant enzymes were purified by affinity and size-exclusion chromatography (Supplemental Figure S1). Xylose isomerase had a molecular mass of 175 kDa; the calculated molecular mass of the subunit is 49.3 kDa, indicating a homotetrameric structure. The enzyme catalyzed the isomerization of D-xylose to xylulose showing a specific activity of 4.4 U/mg and a Km value for D-xylose of 32 mM (Supplemental Figure S2). With D-glucose as a substrate, the enzyme showed a 57-fold lower catalytic efficiency and with L-arabinose no activity (< 1%, at 100 mM) could be measured.

The homotetrameric structure of the *H. utahensis* enzyme and its significant higher catalytic efficiency of isomerization of D-xylose over D-glucose are typical features of most bacterial xylose isomerases as given in BRENDA database (https://www.brenda-enzymes.org/). It should be noted that despite their low catalytic efficiency for D-glucose, xylose isomerases of many bacteria and fungi have been characterized due to their application as "glucose isomerases" in the isomerization of D-glucose to D-fructose as part of the important biotechnological process of starch saccharification generating the sweetener high-fructose corn syrup (Bhosale et al. 1996).

Xylulokinase showed a molecular mass of 133 kDa with a calculated subunit size of 55.1 kDa indicating a homodimeric structure. In bacteria both homodimeric and homotetrameric xylulokinases have been reported (BRENDA database). The *H. utahensis* enzyme catalyzed the ATP-dependent phosphorylation of xylulose with a specific activity of 93.3 U/mg; the apparent Km values for xylulose and ATP were 0.31 mM and 5.68 mM, respectively. L-Ribulose was not phosphorylated at significant rates (< 1%, at 50 mM).

BlastP analyses with xylose isomerase and xylulokinase of *H. utahensis* each revealed hits with high sequence identity only in other *Halorhabdus* species, i.e., *H. tiamatea* (91% identity, xylose isomerase; 93%, xylulokinase) and *Halorhabdus* spec. H27 (86% identity, for each enzyme) suggesting that these haloarchaea degrade D-xylose also via the bacterial-type pathway to xylulose-5-phosphate (Table 1). No homologs of these genes were found in *Halorhabdus rudnickae*, which is in accordance with the report that this *Halorhabdus* strain is not able to grow on D-xylose (Albuquerque et al. 2016). Further, xylose isomerase and xylulokinase were not found in any other archaeal species.

Sequence comparison and phylogenetic affiliation of xylose isomerase from *H. utahensis*

Xylose isomerase of *H. utahensis* showed highest sequence identity with xylose isomerases of the bacteria *Geobacillus stearothermophilus* (63%), *Thermotoga* species (58%), *Bacteroides* species (47%), and of the fungus *Piromyces* (46%); lower identities were found with the xylose isomerases of *Thermus thermophilus* and *Streptomyces* species (21–23%). Xylose isomerase of *Piromyces* and close homologs, e.g., from firmicutes and *Bacteroides* species, were characterized as class II xylose isomerases. Class II enzymes contain an extended N-terminal region and three long loop insertions, which are missing in class I enzymes (Kim et al. 2001; Son et al. 2018). These features are also present in xylose isomerase of *H. utahensis* classifying the enzyme as class II xylose isomerase. A sequence alignment of xylose isomerase of *H.*

Table 1 Enzymes and their encoding genes of bacterial-type degradation pathways of D-xylose, L-arabinose and D-ribose and of the non-oxidative pentosephosphate pathway in *Halorhabdus* species

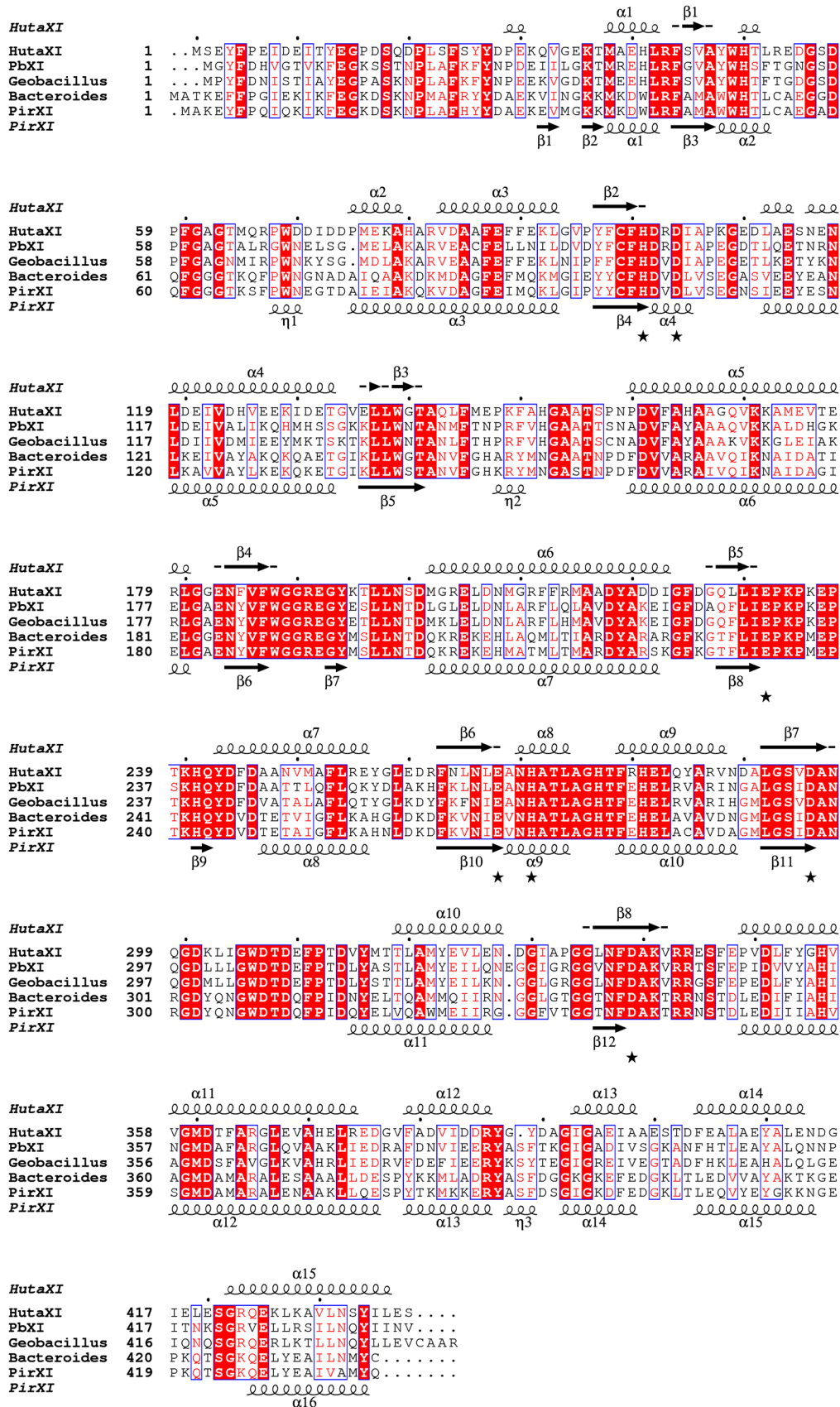| Enzyme name	*H. utahensis*	*H. tiamatea*	*H. rudnickae*	*Halorhabdus* spec. H27
Xylose isomerase	Huta_2443	HTIA_2228	–	WP_136689821
Xylulokinase	Huta_2446	HTIA_2231	–	WP_136689820
Arabinose isomerase	Huta_1154	HTIA_1046 HTIA_p2910	–	WP_136689493
Ribulokinase	Huta_1150	HTIA_1042 HTIA_p2892	–	WP_136689520
L-Ribulose-5-phosphate-4-epimerase	Huta_1149	HTIA_1041 HTIA_p2891	–	WP_136689521
Ribokinase	–	HTIA_0439	WP_135662271	WP_136687548
Ribose-5-phosphate isomerase	Huta_0832	HTIA_0710	WP_135665987	WP_136689787
D-Ribulose-5-phosphate-3-epimerase	Huta_0833	HTIA_0711	WP_135665983	WP_136689785
Transaldolase	Huta_0859	HTIA_0717	WP_135665975	WP_136687890
Transketolase	Huta_0861 Huta_0860	HTIA_0719 HTIA_0718	WP_135665971 WP_167880040 WP_135665973	WP_169051793 WP_136687892 WP_136687891

```
                                                            α1        β1
HutaXI                                              ϙϙ    ϙϙϙϙϙ  ···>    ϙϙ
HutaXI        1  ..MSEYFPEIDEITTYEGPDSQDPLSFSYYDPEKQVGEKTMAEHLRFSVAYWHTLREDGSD
PbXI          1  ...MGYFDHVGTVKFEGKSSTNPLAFKFYNPDEIILGKTMREHLRFGVAYWHSFTGNGSD
Geobacillus   1  ...MPYFDNISTIAYEGPASKNPLAFKFYNPEEKVGDKTMEEHLRFSVAYWHTFTGDGSD
Bacteroides   1  MATKEFFPGIEKIKFEGKDSKNPMAFRYYDAEKVINGKKMKDWLRFAMAWWHTLCAEGGD
PirXI         1  .MAKEYFPQIQKIKFEGKDSKNPLAFHYYDAEKEVMGKKMKDWLRFAMAWWHTLCAEGAD
PirXI            ──>          ──>   ϙϙϙϙϙ  ──>  ϙϙϙϙϙ
                 β1           β2    α1     β3   α2

                                         α2              α3              β2
HutaXI                                 ϙϙϙϙϙ      ϙϙϙϙϙϙϙϙϙϙ       ·──> ·
HutaXI       59  PFGAGTMQRPWDDIDDPMEKAHARVDAAFEFFEKLGVPYFCFHDRDIAPKGEDLAESNEN
PbXI         58  PFGAGTALRGWNELSG.MELAKARVEACFELLNILDVDYFCFHDRDIAPEGDTLQETNRN
Geobacillus  58  PFGAGNMIRPWNKYSG.MDLAKARVEAAFEFFEKLNIPFFCFHDVDIAPEGETLKETYKN
Bacteroides  61  QFGGGTKQFPWNGNADAIQAAKDKMDAGFEFMQKMGIEYYCFHDVDLVSEGASVEEYEAN
PirXI        60  QFGGGTKSFPWNEGTDAIEIAKQKVDAGFEIMQKLGIPYYCFHDVDLVSEGNSIEEYESN
PirXI            ϙϙϙ           ϙϙϙϙϙϙϙϙϙϙϙϙ             ϙϙϙϙ      ϙϙϙϙϙϙϙϙ
                 η1             α3                      β4  α4
                                                              ★   ★

                              α4              β3                      α5
HutaXI            ϙϙϙϙϙϙϙϙϙϙ  ϙϙϙϙϙϙϙϙϙ  ·──>     ·     ϙϙϙϙϙϙϙϙϙϙϙϙϙϙϙϙϙϙϙϙ
HutaXI      119  LDEIVDHVEEKIDETGVELLWGTAQLFMEPKFAHGAATSPNPDVFAHAAGQVKKAMEVTE
PbXI        117  LDEIVALIKQHMHSSGKKLLWNTANMFTNPRFVHGAATTSNADVFAYAAAQVKKALDHGK
Geobacillus 117  LDIIVDMIEEYMKTSKTKLLWNTANLFTHPRFVHGAATSCNADVFAYAAAKVKKGLEIAK
Bacteroides 121  LKEIVAYAKQKQAETGIKLLWGTANVFGHARYMNGAATNPDFDVVARAAVQIKNAIDATI
PirXI       120  LKAVVAYLKEKQKETGIKLLWSTANVFGHKRYMNGASTNPDFDVVARAAIVQIKNAIDAGI
PirXI            ϙϙϙϙϙϙϙϙϙϙϙϙϙϙϙ         ──────>           ϙϙϙ      ϙϙϙϙϙϙϙϙϙϙϙϙϙϙϙϙϙ
                 α5                       β5                 η2              α6

                         β4                          α6                   β5
HutaXI            ϙϙ  ·──>  ·          ϙϙϙϙϙϙϙϙϙϙϙϙϙϙϙϙϙϙϙϙϙϙ        ·──>  ·
HutaXI      179  RLGGENFVFWGGREGYKTLLNSDMGRELDNMGRFFRMAADYADDIGFDGQLLIEPKPKEP
PbXI        177  ELGAENYVFWGGREGYESLLNTDLGLELDNLARFLQLAVDYAKEIGFDAQFLIEPKPKEP
Geobacillus 177  RLGAENYVFWGGREGYMSLLNTDMKLELDNLARFLHMAVDYAKEIGFDGQFLIEPKPKEP
Bacteroides 181  ELGGENYVFWGGREGYMSLLNTDQKREKEHLAQMLTIARDYARARGFKGTFLIEPKPMEP
PirXI       180  ELGAENYVFWGGREGYMSLLNTDQKREKEHMATMLTMARDYARSKGFKGTFLIEPKPMEP
PirXI            ϙϙ    ──>       ──>          ϙϙϙϙϙϙϙϙϙϙϙϙϙϙϙϙϙϙϙϙϙϙϙ      ──>
                 β6       β7                    α7                        β8
                                                                            ★

                         α7                   β6         α8         α9          β7
HutaXI            ϙϙϙϙϙϙϙϙϙϙϙϙϙϙϙϙϙϙ        ──>  ·     ϙϙϙϙϙ     ϙϙϙϙϙϙϙϙϙϙ        ──> ·
HutaXI      239  TKHQYDFDAANVMAFLREYGLEDRFNLNLEANHATLAGHTFRHELQYARVNDALGSVDAN
PbXI        237  SKHQYDFDAATTLQFLQKYDLAKHFKLNLEANHATLAGHTFEHELRVARINGALGSIDAN
Geobacillus 237  TKHQYDFDVATALAFLQTYGLKDYFKFNIEANHATLAGHTFEHELRVARIHGMLGSVDAN
Bacteroides 241  TKHQYDVDTETVIGFLKAHGLDKDFKVNIEVNHATLAGHTFEHELAVAVDNGMLGSIDAN
PirXI       240  TKHQYDVDTETAIGFLKAHNLDKDFKVNIEVNHATLAGHTFEHELACAVDAGMLGSIDAN
PirXI            ──>       ϙϙϙϙϙϙϙϙϙϙϙϙϙ       ──>  ·   ϙϙϙϙϙ     ϙϙϙϙϙϙϙϙϙ        ──>
                 β9         α8                   β10     α9          α10         β11
                                                   ★    ★                          ★

                                           α10                    β8
HutaXI                                   ϙϙϙϙϙϙϙϙϙϙ           ·──>  ·         ϙϙϙϙϙϙϙϙϙϙ
HutaXI      299  QGDKLIGWDTDEFPTDVYMTTLAMYEVLEN.DGIAPGGLNFDAKVRRESFEPVDLFYGHV
PbXI        297  QGDLLLGWDTDEFPTDLYASTLAMYEILQNEGGIGRGGVNFDAKVRRTSFEPIDVVYAHI
Geobacillus 297  QGDMLLGWDTDEFPTDLYSTTLAMYEILKN.GGLGRGGLNFDAKVRRGSFEPEDLFYAHI
Bacteroides 301  RGDYQNGWDTDQFPIDNYELTQAMMQIIRN.GGLGTGGTNFDAKTRRNSTDLEDIFIAHI
PirXI       300  RGDYQNGWDTDQFPIDQYELVQAWMEIIRG.GGFVTGGTNFDAKTRRNSTDLEDIIIAHV
PirXI            ϙϙϙϙϙϙϙϙϙϙϙϙ                          ──>
                 α11                                  β12
                                                        ★

                    α11                     α12            α13         α14
HutaXI            ϙϙϙϙϙϙϙϙϙϙϙϙϙϙϙϙϙϙ       ϙϙϙϙϙϙϙϙϙ      ϙϙϙϙϙϙϙ      ϙϙϙϙϙϙϙϙϙ
HutaXI      358  VGMDTFARGLEVAHELREDGVFADVIDDRYG.YDAGIGAEIAAESTDFEALAEYALENDG
PbXI        357  NGMDAFARGIQVAAKLIEDRAFDNVIEERYASFTKGIGADIVSGKANFHTLEAYALQNNP
Geobacillus 356  AGMDSFAVGLKVAHRLIEDRVFDEFIEERYKSYTEGIGREIVEGTADFHKLEAHALQLGE
Bacteroides 360  RGDYQNGMDAMARALESAAALLDESPYKKMLADRYASFDGGKGKEFEDGKLTLEDVVAYAKTKGE
PirXI       359  SGMDAMARALENAAKLLQESPYTKMKKERYASFDSGIGKDFEDGKLTLEQVYEYGKKNGE
PirXI            ϙϙϙϙϙϙϙϙϙϙϙϙϙϙϙϙϙϙϙ      ϙϙϙϙϙϙϙϙϙ      ϙϙϙ  ϙϙϙϙϙϙϙ      ϙϙϙϙϙϙϙϙϙϙ
                 α12                       α13           η3   α14           α15

                        α15
HutaXI            ϙϙϙϙϙϙϙϙϙϙϙϙϙϙϙϙ
HutaXI      417  IELESGRQEKLKAVLNSYILES....
PbXI        417  ITNKSGRVELLRSILNQYIINV....
Geobacillus 416  IQNQSGRQERLKTLLNQYLLEVCAAR
Bacteroides 420  PKQTSGKQELYEAILNMYC.......
PirXI       419  PKQTSGKQELYEAIVAMYQ.......
PirXI            ϙϙϙϙϙϙϙϙϙϙϙϙ
                 α16
```

utahensis with selected class II sequences is shown in Fig. 3. The predicted secondary structure of xylose isomerase from *H. utahensis* matches well with the structure elements concluded from crystal structure of the *Piromyces* enzyme (Son et al. 2018). Further, residues involved in the catalysis are conserved in the haloarchaeal enzyme.

A phylogenetic analysis was performed with xylose isomerase of *H. utahensis* and selected enzymes of class I and class II xylose isomerases (Fig. 4). The tree topology demonstrates that xylose isomerases cluster according to their affiliation to class I or II enzymes. Class I comprise xyloses isomerases from *Streptomyces* and *Thermus* species and class II xylose isomerases from firmicutes, *Thermotoga* species, proteobacteria, bacteroides, *Hordeum vulgare* and fungi. Xylose isomerase from *H. utahensis* belongs to the class II cluster in accordance with the sequence alignment (Fig. 3). Within the class II cluster, the haloarchaeal enzymes form a sub-cluster together with firmicutes and *Thermotoga* species. Together, the finding that the xylose isomerase of *H. utahensis* is closely related to firmicutes/*Thermotoga* xylose isomerases, and the absence of xylose isomerases in any other archaeal species suggests that xylose isomerase in *Halorhabdus* species has been acquired from firmicutes via lateral gene transfer.

L-Arabinose degradation to xylulose-5-phosphate in *H. utahensis*

H. utahensis grew on L-arabinose with a doubling time of 18 h up to an optical density at 600 nm of 1.0 (Fig. 5a). In cell extracts of L-arabinose-grown cells, activities of arabinose dehydrogenase and α-ketoglutarate dehydrogenase could not be detected excluding an oxidative pathway of L-arabinose degradation in *H. utahensis*. Instead, the organism contains genes that encode putative arabinose isomerase (Huta_1154), ribulokinase (Huta_1150) and L-ribulose-5-phosphate-4-epimerase (Huta_1149), i.e., enzymes of the classical non-oxidative L-arabinose degradation pathway found in most bacteria. (Fig. 5b).

Transcription of Huta_1154 and Huta_1150 was followed by Northern blot analyses using RNA from cells grown on D-xylose, L-arabinose, D-ribose and D-glucose. A signal at about 1600 nucleotides was detected in all RNAs using a Huta_1154 specific probe that matches well to the gene length of 1488 nucleotides (not shown). With a probe against Huta_1150, two signals were detected in pentose- and glucose-grown cells, at about 2200 and 1300 nucleotides, indicating cotranscription of Huta_1150 (1539 nucleotides) and Huta_1149 (648 nucleotides), as well as single transcription of Huta_1150 (Supplemental Figure S3). The data indicate that the three genes are constitutively expressed during growth on D-glucose and the three pentoses. In contrast, L-arabinose degradation in bacteria has been reported to be specifically regulated by L-arabinose (Luo et al. 2014).

Huta_1154 was expressed and the recombinant arabinose isomerase was purified (Supplemental Figure S1) as 322 kDa enzyme, the calculated molecular mass of the subunits is 55.4 kDa indicating a homohexameric structure. The specific activity was 129.5 U/mg; the apparent Km value was 254.6 mM for L-arabinose. No activity was measured with D-galactose, D-arabinose, D-ribose and D-xylose (tested at 10 and 100 mM).

The oligomerization of arabinose isomerase of *H. utahensis* as homohexamer has been reported for few bacterial and eukaryal enzymes, e.g., from *E. coli* (Patrick and Lee 1969) and from *Arthrobacter* sp. (Wanarska and Kur 2012); however, the majority of arabinose isomerases, e.g., from *Bacillus* species, were characterized as homotetrameric enzymes (Wanarska and Kur 2012).

The arabinose isomerase of *H. utahensis* is highly specific for the isomerization of L-arabinose showing no activity with D-galactose. Thus, the enzyme differs from most characterized arabinose isomerases from eukarya and bacteria which catalyze—in addition to L-arabinose—the isomerization of D-galactose to D-tagatose. Since D-tagatose is used as a low-calorie sugar substitute in food industry, arabinose isomerases are well-studied enzymes in biotechnology (Kim 2004). However, few bacterial arabinose isomerases have been described, e.g., from *Bacillus* species, that also have a high specificity for L-arabinose over D-galactose as the *Halorhabdus* enzyme (Li et al. 2011; Prabhu et al. 2008).

Homologs of arabinose isomerase were found in other *Halorhabdus* species, e.g., *Halorhabdus tiamatea* and *Halorhabdus* spec. H27, rather than in *Halorhabdus rudnickae* (Table 1). Further, the haloarchaeal arabinose isomerase shows high sequence identity (53%) to homologs of bacteria, e.g., *E. coli* and *Bacillus subtilis*.

The recombinant ribulokinase encoded by Huta_1150 was purified (Supplemental Figure S1) as enzyme of 348 kDa; the calculated molecular mass of subunit is 56.1 kDa indicating a homohexameric structure. The enzyme catalyzed the ATP-dependent phosphorylation of L-ribulose with a specific activity of 60.5 U/mg; the apparent Km values of L-ribulose and ATP were 0.55 mM and 4.2 mM, respectively; D-xylose was not used as substrate. Ribulokinase

Fig. 4 Phylogenetic relationship of xylose isomerase from *Halorhabdus* species and class I and class II xylose isomerases from bacteria and eukarya. *H. utahensis*, C7NMH0; *H. tiamatea*, S6CUC8; *Halorhabdus* sp. H27, WP_136689821; *Lactobacillus reuteri*, Q5QG16 (Staudigl et al. 2014); *Thermoanaerobacterium thermosulfurigenes*, P19148; *Thermotoga neapolitana*, P45687; *Thermotoga maritima*, Q9X1Z5 (Bandlish et al. 2002); *Geobacillus stearothermophilus*, P54273; *Caldicoprobacter algeriensis*, A0A481U6W5 (Neifar et al. 2019); *Paenibacillus* sp. R4, 6INT; *E. coli*, P00944; *Vibrio* sp., C7G532 (Umemoto et al. 2012); *Orpinomyces* sp., B7SLY1 (Madhavan et al. 2009); *Piromyces* sp., Q9P8C9 (Son et al. 2018); *Bacteroides thetaiotaomicron*, Q8A9M2 (Cho et al. 2013); *Hordeum vulgare*, Q40082; *Thermus caldophilus*, P56681; *Thermus thermophiles*, P26997; *Streptomyces olivochromogenes*, P15587; *Streptomyces rubiginosus*, P24300; *Actinoplanes missouriensis*, E6YBC0 (Wang et al. 2011)
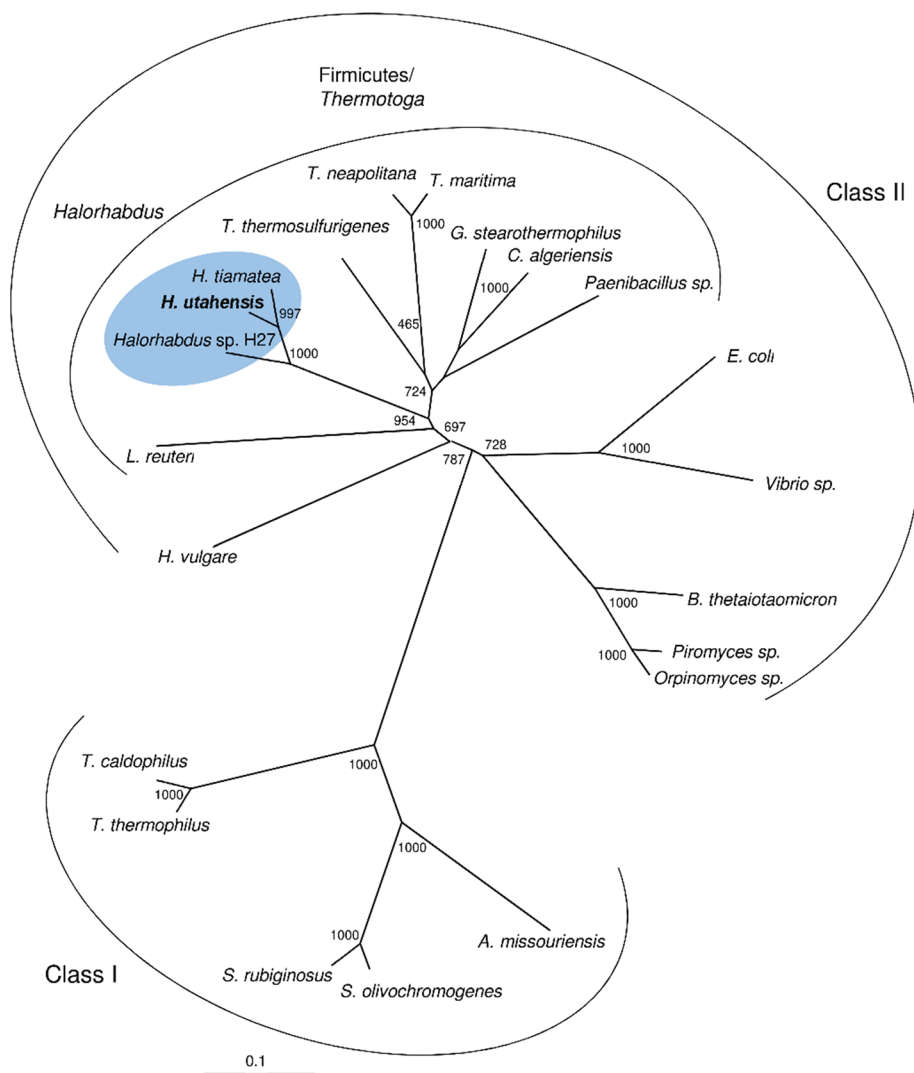
shows high sequence identity to homologs in *H. tiamatea* (95% identity) and *Halorhabdus* spec. H27 (83%) rather than in *H. rudnickae* (Table 1).

Huta_1149 encoding L-ribulose-5-phosphate-4-epimerase forms a cotranscript with Huta_1150 (Fig. 5, Supplemental Figure S3). In bacteria, L-ribulose-5-phosphate-4-epimerases catalyze the conversion of ribulose-5-phosphate to D-xylulose-5-phosphate. Putative homologs of this enzyme were only found in *Halorhabdus* species *H. tiamatea* and *Halorhabdus* sp. H27 (Table 1). Together, we propose that these *Halorhabdus* species degrade L-arabinose via the classical bacterial-type pathway.

D-Ribose degradation to xylulose-5-phosphate in Halorhabdus species

H. utahensis grew on D-ribose with a doubling time of 29 h up to optical densities at 600 nm of about 1.6 (Fig. 6). A gene encoding ribonate dehydratase, the key enzyme of oxidative D-ribose degradation in *Haloarcula* species, is not present in genomes of *Halorhabdus* species. Instead, genes were identified that encode putative enzymes of the classical non-oxidative D-ribose degradation pathway operative in most bacteria. In the genome of *H. utahensis* two clustered genes, Huta_0832 and Huta_0833, encoding putative ribose-5-phosphate isomerase and D-ribulose-5-phosphate-3-epimerase are annotated; a gene homologous to ribokinase from *E. coli* could not be identified. In contrast to *H. utahensis*, we found that the *Halorhabdus* species *H. tiamatea, Halorhabdus* sp. H27 and *H. rudnickae* each contain a bacterial type ribokinase gene in addition to the genes encoding ribose-5-phosphate isomerase and D-ribulose-5-phosphate-3-epimerase (Fig. 6; Table 1).

HTIA_0439 encoding putative ribokinase in *H. tiamatea* was overexpressed and the recombinant protein was purified. Ribokinase was characterized as dimeric protein of 70 kDa composed of 31.3 kDa subunits (Supplemental Figure S4). The enzyme catalyzed the ATP-dependent phosphorylation

Fig. 5 L-Arabinose degradation in *Halorhabdus utahensis*. **a** Growth of *H. utahensis* on L-arabinose. Growth was performed at 37 °C on 15 mM L-arabinose in synthetic medium (filled circle); consumption of L-arabinose (filled square). **b** Genome organization of Huta_1154, Huta_1150 and Huta_1149 encoding putative arabinose isomerase, ribulokinase and L-ribulose-5-phosphate-4-epimerase (grey arrows)
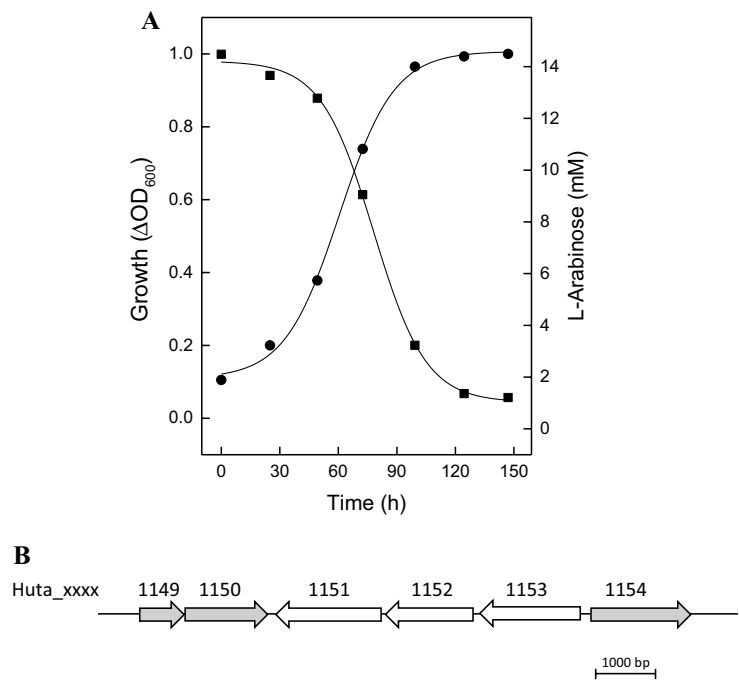
of D-ribose with a specific activity of 34.5 U/mg and apparent Km values of D-ribose and ATP of 0.6 mM and 0.1 mM, respectively (Fig. 7).

Despite the absence of a bacterial ribokinase gene in *H. utahensis*, D-ribose-grown cells showed low ribokinase activity (~ 1 mU/mg). To identify the encoding gene we purified ribokinase activity up to 1300-fold (Supplemental Figure S5). The purified ribokinase showed a single subunit on SDS-PAGE of 75 kDa and by MALDI-TOF analysis Huta_1150 was identified as the encoding gene; this gene encodes ribulokinase involved in L-arabinose degradation (see above). We reanalyzed the kinetic properties of ribulokinase and found that it catalyzed the phosphorylation of D-ribose with a specific activity of 1.3 U/mg. We propose that in *H. utahensis* the phosphorylation of D-ribose is catalyzed by ribulokinase that functionally replaces the missing ribokinase as first enzyme of the D-ribose degradation pathway.

Sequence comparison and phylogenetic affiliation of ribokinase from *H. tiamatea*

The ribokinase from *H. tiamatea* shows significant sequence identity with putative ribokinases from the *Halorhabdus* species *H. rudnickae* (59%) and *Halorhabdus* sp. H27 (78%) and at lower identity from other archaea, e.g., *Sulfolobus solfataricus* (29%) and *Ferroplasma acidiphilum* (32%). *H. tiamatea* ribokinase also shows significant sequence identity with characterized ribokinases from bacteria and eukarya, including *Escherichia coli* (37%), *Staphylococcus aureus* (34%), human (30%) and *Arabidopsis thaliana*

(28%). A sequence alignment of ribokinase of *H. tiamatea* and selected ribokinases characterized from bacteria and eukarya, and the putative archaeal ribokinase from *S. solfataricus* is shown in Fig. 8. The predicted secondary structure of ribokinase from *H. tiamatea* matches well with the structure elements of *E. coli* ribokinase (Andersson and Mowbray 2002). Further, residues that are involved in binding of D-ribose based on crystal structures of *E. coli* and *A. thaliana* are conserved in the haloarchaeal enzyme (Andersson and Mowbray 2002; Kang et al. 2019). Ribokinases belong to the PfkB family of carbohydrate kinases (Park and Gupta 2008) and sequences of this family contain the two typical sequence pattern of PfkB family (Fig. 8). Further, the alignment demonstrates the similarity of characterized ribokinases and the putative ribokinase from *S. solfataricus*. The residues for D-ribose binding are conserved in *Sulfolobus* enzyme suggesting that it also shows ribokinase activity; yet, its catalytic activity and functional involvement in D-ribose phosphorylation as part of a D-ribose degradation pathway in *Sulfolobus* have to be demonstrated.

Ribokinase from *H. tiamatea* and archaeal homologs from other *Halorhabdus* species and from *S. solfataricus* and *F. acidiphilum* are members of the ribokinase superfamily (PfkB family of carbohydrate kinases). A phylogenetic relationship between ribokinases and four selected families of the ribokinase superfamily is shown in Fig. 9. The tree topology shows that ribokinases and the members of other families each form a distinct cluster according to their various kinase functions as follows: (1) the ribokinase cluster includes characterized and putative enzymes from eukarya, bacteria and archaea, whereby the *Halorhabdus tiamatea*
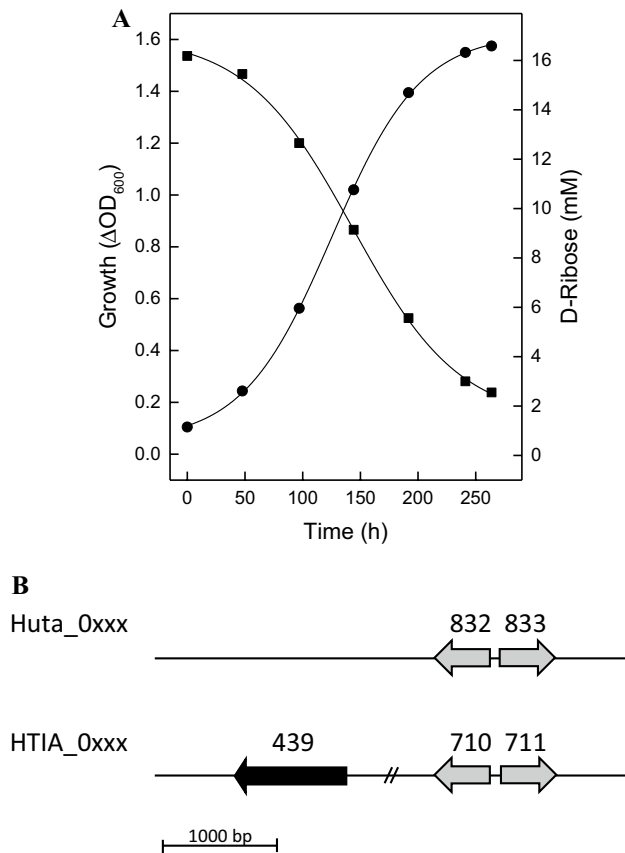
B

Huta_0xxx

HTIA_0xxx

Fig. 6 D-Ribose degradation in *Halorhabdus* species *H. utahensis* and *H. tiamatea*. **a** Growth of *H. utahensis* was performed at 37 °C on 15 mM D-ribose in synthetic medium (filled circle); consumption of D-ribose (filled square). **b** Genomic view of genes involved in D-ribose degradation in *H. utahensis* and *H. tiamatea*. A homologous gene of HTIA_0439 (black arrow) encoding ribokinase of *H. tiamatea* is absent in *H. utahensis*. HTIA_0710 and Huta_0832 encode ribose-5-phosphate isomerase and HTIA_0711 and Huta_0833 encode D-ribulose-5-phosphate-3-epimerase (grey arrows)

enzyme represents the first characterized ribokinase in the archaeal domain. (2) The phosphofructokinase/ribose-1-phosphate kinase cluster includes archaeal ADP- and ATP-dependent ribose-1-phosphate kinases from *T. kodakarensis* and *P. calidifontis* and archaeal ATP-dependent phosphofructokinases from *A. pernix* and *D. amylolyticus*. Further, putative proteins from the haloarchaeon *H. hispanica*, and from *T. tenax* belong to this cluster. (3) The glucokinase/ phosphofructokinase cluster includes ADP-dependent glucokinases and phosphofructokinases from hyperthermophilic euryarchaeota, *P. furiosus* and *M. jannaschii*, fructokinases from the bacteria *E. coli* and *Z. mobilis* and ATP-dependent glucokinases from the crenarchaeota *A. pernix* and *T. tenax*. (4) The nucleoside kinase/adenosine kinase cluster includes adenosine kinase from the bacterium *M. tuberculosis*, a nucleoside kinase from the archaeon *M. jannaschii* and a putative homolog from *T. acidophilum*. (5) The KDG kinase cluster includes KDG kinases from the bacteria *T. maritima* and *T. thermophilus*, from the archaea *S. solfataricus* and *T. tenax* and from the haloarchaeon *H. volcanii*.

A similar topology of members of the ribokinase superfamily from archaea, bacteria and eukarya has been reported previously (Aziz et al. 2018; Hansen et al. 2007). With the characterization of the ribokinase of *H. tiamatea*, we expand the ribokinase cluster by the first characterized archaeal member.

Huta_0832 of *H. utahensis* encodes a putative ribose-5-phosphate isomerase of the RpiA family. Transcript analysis of Huta_0832 (687 nucleotides) was performed by Northern blotting with RNA from cells grown on D-xylose, D-ribose and L-arabinose as compared to D-glucose. A specific transcript signal at 800 nucleotides could be detected in D-glucose- and pentose-grown cells indicating that Huta_0832 was constitutively expressed on these sugars (Supplemental Figure S6). Huta_0832 was overexpressed

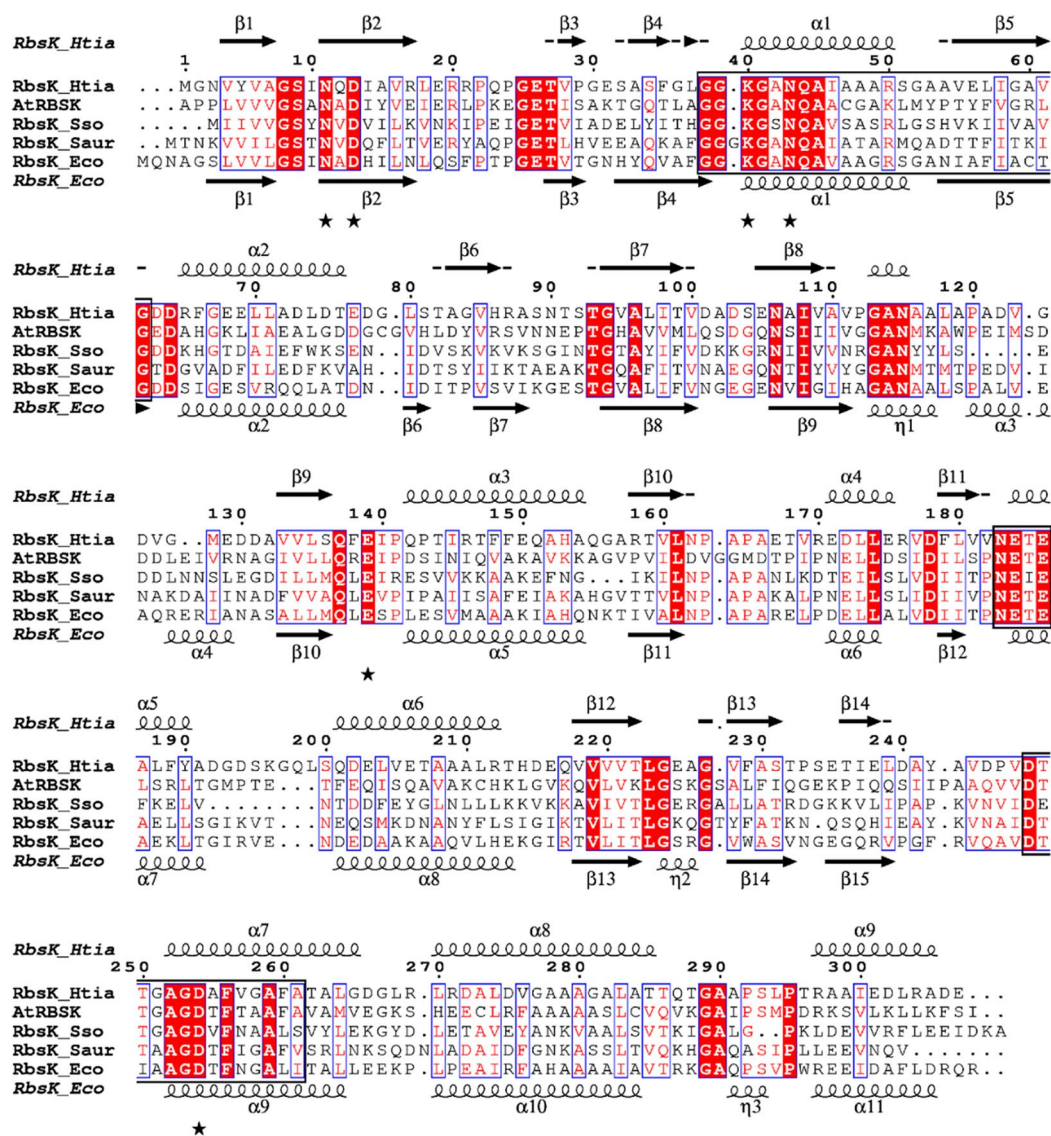**Fig. 7** Rate dependence of ribokinase of *H. tiamatea* on the concentrations of ribose and ATP
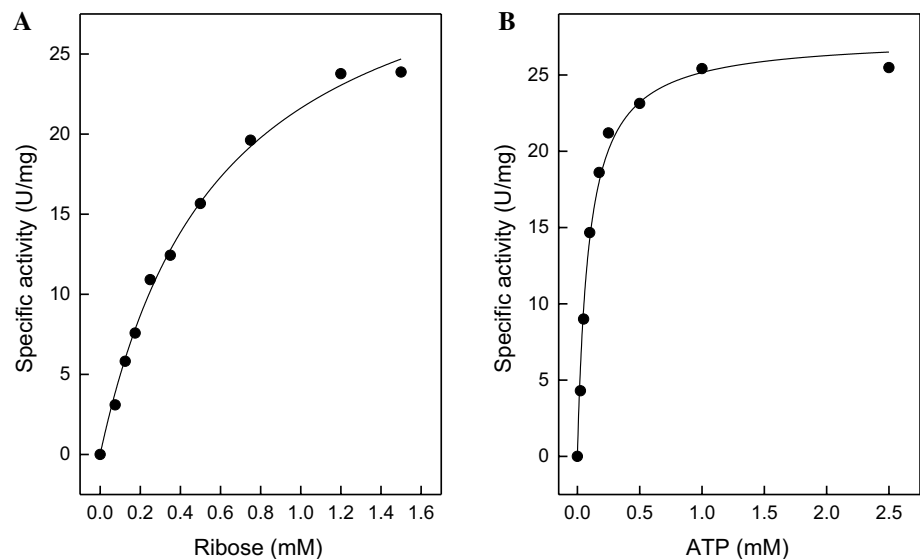
Fig. 8 Amino acid sequence alignment of ribokinase from *H. tiamatea* with selected characterized and putative ribokinases from bacteria, archaea and eukarya. Highly conserved residues are shown in red and boxed in blue; strictly conserved residues are shown with a red background. The two signatures (PDOC00504) of pfkB family of carbohydrate kinases and the typical ribokinase family NXXE motif (Park and Gupta 2008) are boxed. Predicted secondary structure elements of *H. tiamatea* ribokinase match well with the structure-based secondary structure elements of *E. coli* ribokinase (Andersson and Mowbray 2002). Conserved amino acids involved in ribose binding are marked by asterisks according to the structures from *E. coli* and *Arabidopsis thaliana* (Andersson and Mowbray 2002; Kang et al. 2019). PDB identifier: *E. coli*, 1GQT; *A. thaliana*, the first 69 residues are not shown, 6ILT; *S. aureus*, 3RY7. UniProt entry number: *H. tiamatea*, HTIA_0439, C7NMH0; *Sulfolobus solfataricus*, Q981E2

and the purified enzyme was characterized as 98.5 kDa homotetrameric protein composed of 23.9 kDa subunits (Supplemental Figure S1). The enzyme showed a specific activity of 291.6 U/mg and a Km value of D-ribose-5-phosphate of 7.64 mM; D-glucose and D-xylose were not used. Huta_0833 encodes a putative D-ribulose-5-phosphate-3-epimerase that in bacteria catalyzes the conversion of D-ribulose-5-phosphate to D-xylulose-5-phosphate. Homologs of ribose-5-phosphate isomerase and D-ribulose-5-phosphate-3-epimerase from *H. utahensis* were also found

in *Halorhabdus* species *H. tiamatea*, *H. rudnickae* and *Halorhabdus* strain H27 (Table 1).

In summary, we conclude that *Halorhabdus utahensis* degrades the pentoses via the bacterial-type pathways yielding D-xylulose-5-phosphate. A comparative analysis of genomes of four *Halorhabdus* species, *H. utahensis*, *H. tiamatea*, *H. rudnickae* and *Halorhabdus* strain H27 revealed the presence of all genes of the bacterial pentose degradation pathways with few variations: *H. utahensis* does not contain ribokinase but rather utilizes
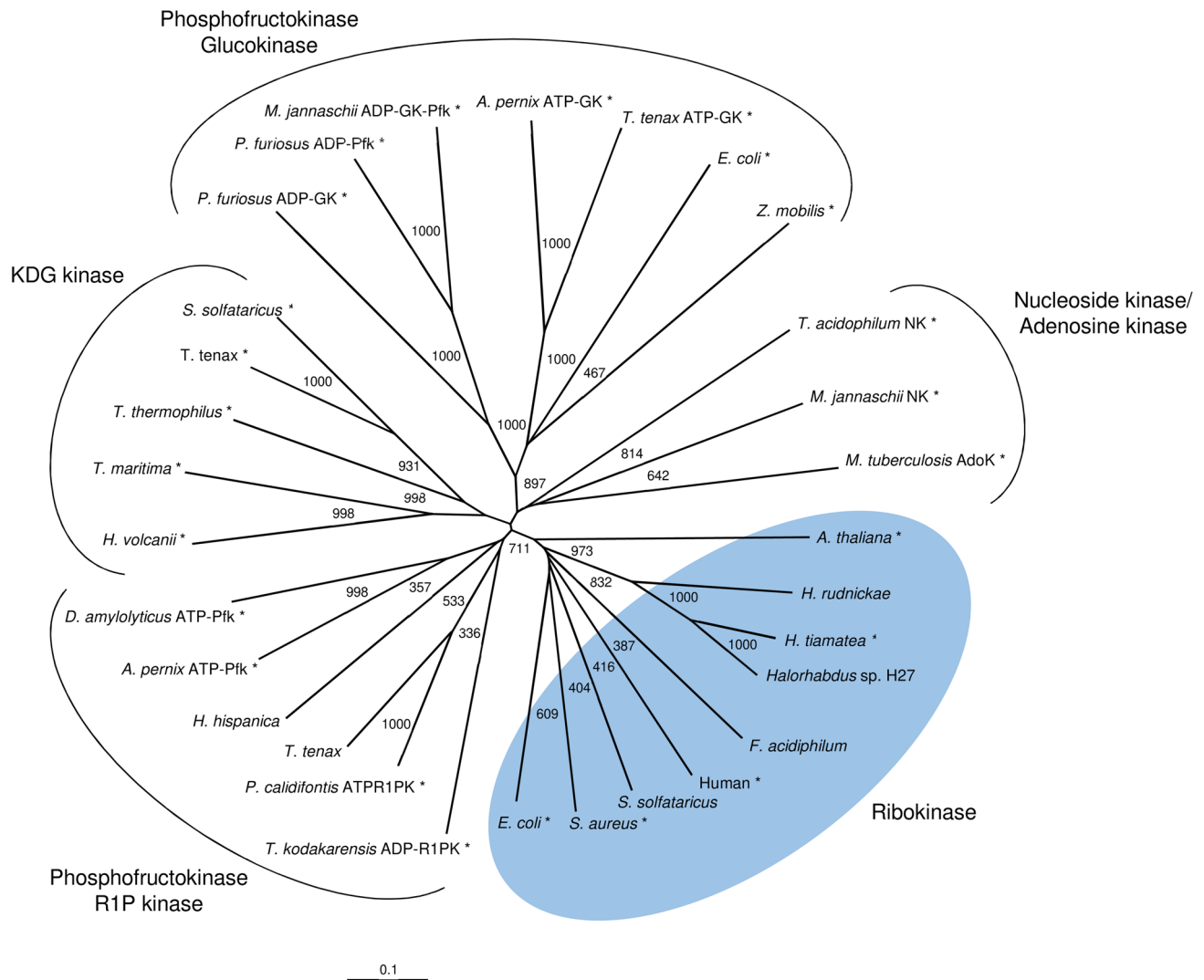
Fig. 9 Phylogenetic relationship of ribokinase from *H. tiamatea* with ribokinases from bacteria, eukarya and archaea and related members of the ribokinase superfamily. Ribokinase: *Halorhabdus tiamatea*, HTIA_0439; *Halorhabdus rudnickae*, WP_135662271; *Halorhabdus* sp. H27, WP_136687548; *Arabidopsis thaliana*, A1A6H3; *Ferroplasma acidiphilum*, A0A1V0N6I9; *Sulfolobus solfataricus*, SSO0004; Human, Q9H477; *E. coli*, P0A9J6; *Staphylococcus aureus*, A0A0H2WZY4; Nucleoside/adenosine kinase: *Thermoplasma acidophilum*, Ta0880; *Methanocaldococcus jannaschii*, MJ0406; *Mycobacterium tuberculosis*, P9WID5; Phosphofructokinase/ribose-1-phosphate kinase: *Desulfurococcus amylolyticus*, WP_042667458 (Hansen and Schönheit 2000); *Aeropyrum pernix*, Ape0012 (Hansen and Schönheit 2001); *Thermoproteus tenax*, TTX_1882; *Pyrobaculum calidifontis*, Pcal 0041 (Aziz et al. 2018); *Haloterrigena hispanica*, A0A1G6RMF8; *Thermococcus kodakarensis*, TK2029 (Aono et al. 2015); Glucokinase/phosphofructokinase: *T. tenax*, TTX0060 (Dörr et al. 2003); *A. pernix*, Ape2091; *Zymomonas mobilis*, Q03417 (King et al. 1996); *E. coli*, P23917; *M. jannaschii*, MJ1604; *Pyrococcus furiosus*, PF1784 (ADP-Pfk); *P. furiosus*, PF0312 (ADP-GK); 2-Keto-3-deoxygluconate kinase: *Haloferax volcanii*, HVO_0549; *Thermotoga maritima*, Q9WXS2 (Mathews et al. 2008); *Thermus thermophilus*, Q53W83; *T. tenax*, TTX_1157 (Ahmed et al. 2005); *S. solfataricus*, SSO3195

L-ribulokinase for D-ribose phosphorylation, and the genes of D-xylose and L-arabinose degradation are absent in *H. rudnickae* (Table 1). Further degradation of xylulose-5-phosphate in the *Halorhabdus* species likely involves the enzymes of the non-oxidative branch of the pentose phosphate pathway (NOPP), i.e., D-ribulose-5-phosphate-3-epimerase, ribose-5-phosphate isomerase, transketolase and transaldolase, to generate the glycolytic intermediates fructose-6-phosphate and glyceraldehyde-3-phosphate (Table 1). These intermediates are further oxidized to CO_2 to generate ATP involving enzymes of the Embden–Meyerhof pathway (Anderson et al. 2011), citric acid cycle and respiratory chain. Beside its role in pentose catabolism the NOPP pathway is also involved in the formation of sugar phosphates in anabolism.

Bacterial-type versus archaeal-type of pentose degradation in haloarchaea

In this study, we showed that *Halorhabdus* species degrade pentoses via bacterial-type pathways yielding xylulose-5-phosphate. The exclusive presence of these pathways in *Halorhabdus* species and the absence in other archaea indicate that the pentose degradation pathways have been acquired by *Halorhabdus* from bacteria via horizontal gene transfer. Thus, *Halorhabdus* species utilizing the bacterial-type pentose degradation pathway generating xylulose-5-phosphate differ from other haloarchaea, i.e., *Haloferax* and *Haloarcula* species which degrade pentoses via the archaeal oxidative pathway yielding α-ketoglutarate, an intermediate of the citric acid cycle. The reason why *Halorhabdus* species do not use the oxidative pathway generating α-ketoglutarate might be explained by an incomplete gluconeogenetic pathway reported for *Halorhabdus* species. *Halorhabdus* species lack the enzymes that convert α-ketoglutarate via malate to the central intermediate phosphoenolpyruvate; these include malic enzyme, phosphoenolpyruvate synthetase/pyruvate phosphate dikinase or phosphoenolpyruvate carboxykinase. Thus, utilization of α-ketoglutarate in the anabolism is prevented. In contrast, *Haloferax* and *Haloarcula* species that use the oxidative pathway contain all enzymes of gluconeogenesis, which—together with malic enzyme and phosphoenolpyruvate synthetase—catalyze the conversion of α-ketoglutarate to phosphoenolpyruvate. Thus, we conclude that the utilization of different types of pentose catabolic pathways in haloarchaea is due to the different pathways in the anabolism.

Compliance with ethical standard

Conflict of interest The authors declare that there are no conflicts of interest.

References

Ahmed H, Ettema TJ, Tjaden B, Geerling AC, van der Oost J, Siebers B (2005) The semi-phosphorylative Entner-Doudoroff pathway in hyperthermophilic archaea—a re-evaluation. Biochem J 390:546

Albuquerque L, Kowalewicz-Kulbat M, Drzewiecka D, Staczek P, d'Auria G, Rossello-Mora R, da Costa MS (2016) *Halorhabdus rudnickae* sp. nov., a halophilic archaeon isolated from a salt mine borehole in Poland Syst Appl Microbiol 39:100–105 https://doi.org/10.1016/j.syapm.2015.12.004

Allers T, Barak S, Liddell S, Wardell K, Mevarech M (2010) Improved strains and plasmid vectors for conditional overexpression of His-tagged proteins in *Haloferax volcanii*. Appl Environ Microbiol 76:1759–1769

Anderson I et al (2011) Novel insights into the diversity of catabolic metabolism from ten haloarchaeal genomes. PLoS ONE 6:e20237

Andersson CE, Mowbray SL (2002) Activation of ribokinase by monovalent cations. J Mol Biol 315:409–419

Aono R, Sato T, Imanaka T, Atomi H (2015) A pentose bisphosphate pathway for nucleoside degradation in Archaea. Nat Chem Biol 11:355–360. https://doi.org/10.1038/nchembio.1786

Aziz I, Bibi T, Rashid N, Aono R, Atomi H, Akhtar M (2018) A phosphofructokinase homolog from *Pyrobaculum calidifontis* displays kinase activity towards pyrimidine nucleosides and ribose 1-phosphate. J Bacteriol. https://doi.org/10.1128/JB.00284-18

Bandlish RK, Michael Hess J, Epting KL, Vieille C, Kelly RM (2002) Glucose-to-fructose conversion at high temperatures with xylose (glucose) isomerases from *Streptomyces murinus* and two hyperthermophilic *Thermotoga* species. Biotechnol Bioeng 80:185–194. https://doi.org/10.1002/bit.10362

Bhosale SH, Rao MB, Deshpande VV (1996) Molecular and industrial aspects of glucose isomerase. Microbiol Rev 60:280–300

Brouns SJ et al (2006) Identification of the missing links in prokaryotic pentose oxidation pathways: evidence for enzyme recruitment. J Biol Chem 281:27378–27388

Buchan DW, Minneci F, Nugent TC, Bryson K, Jones DT (2013) Scalable web services for the PSIPRED Protein Analysis Workbench. Nucleic Acids Res 41:W349–W357

Cho JW, Han BG, Park SY, Kim SJ, Kim MD, Lee BI (2013) Overexpression, crystallization and preliminary X-ray crystallographic analysis of a putative xylose isomerase from *Bacteroides thetaiotaomicron*. Acta Crystallogr Sect F Struct Biol Cryst Commun 69:1127–1130. https://doi.org/10.1107/S1744309113023877

Dörr C, Zaparty M, Tjaden B, Brinkmann H, Siebers B (2003) The hexokinase of the hyperthermophile *Thermoproteus tenax*: ATP-dependent hexokinases and ADP-dependent glucokinases, two alternatives for glucose phosphorylation in Archaea. J Biol Chem 278:18744–18753

Hansen T, Arnfors L, Ladenstein R, Schönheit P (2007) The phosphofructokinase-B from *Methanocaldococcus jannaschii* (ORF MJ0406) represents a nucleoside kinase with a broad substrate specifity. Extremophiles 11:105–114

Hansen T, Schönheit P (2000) Purification and properties of the first-identified, archaeal, ATP-dependent 6-phosphofructokinase, an extremely thermophilic non-allosteric enzyme, from the hyperthermophile *Desulfurococcus amylolyticus*. Arch Microbiol 173:103–109

Hansen T, Schönheit P (2001) Sequence, expression, and characterization of the first archaeal ATP-dependent 6-phosphofructokinase, a non-allosteric enzyme related to the phosphofructokinase-B sugar kinase family, from the hyperthermophilic crenarchaeote *Aeropyrum pernix*. Arch Microbiol 177:62–69

Horecker BL (1988) D-Xylulose and D-Xylose. In: Bergmeyer H-U (ed) Methods of Enzymatic Analysis. VCH Verlagsgesellschaft mbH, Weinheim, Third Edition edn, pp 465–473

Johnsen U, Dambeck M, Zaiss H, Fuhrer T, Soppa J, Sauer U, Schönheit P (2009) D-xylose degradation pathway in the halophilic archaeon *Haloferax volcanii*. J Biol Chem 284:27290–27303

Johnsen U, Schönheit P (2004) Novel xylose dehydrogenase in the halophilic archaeon *Haloarcula marismortui*. J Bacteriol 186:6198–6207

Johnsen U, Sutter JM, Reinhardt A, Pickl A, Wang R, Xiang H, Schönheit P (2020) D-Ribose catabolism in archaea: discovery of a novel oxidative pathway in *Haloarcula* species. J Bacteriol. https://doi.org/10.1128/JB.00608-19

Johnsen U, Sutter JM, Zaiss H, Schönheit P (2013) L-Arabinose degradation pathway in the haloarchaeon *Haloferax volcanii* involves a novel type of L-arabinose dehydrogenase. Extremophiles 17:897–909

Kang PA, Oh J, Lee H, Witte CP, Rhee S (2019) Crystal structure and mutational analyses of ribokinase from *Arabidopsis thaliana*. J Struct Biol 206:110–118. https://doi.org/10.1016/j.jsb.2019.02.007

Kim P (2004) Current studies on biological tagatose production using L-arabinose isomerase: a review and future perspective. Appl Microbiol Biotechnol 65:243–249. https://doi.org/10.1007/s00253-004-1665-8

Kim YS et al (2001) Crystallization and preliminary X-ray studies of Trp138Phe/Val185Thr xylose isomerases from *Thermotoga neapolitana* and *Thermoanaerobacterium thermosulfurigenes*. Acta Crystallogr D Biol Crystallogr 57:1686–1688

King K, Phan P, Rellos P, Scopes RK (1996) Overexpression, purification, and generation of a thermostable variant of *Zymomonas mobilis* fructokinase. Protein Expr Purif 7:373–376

Larkin MA et al (2007) Clustal W and Clustal X version 2.0. Bioinformatics 23:2947–2948. https://doi.org/10.1093/bioinformatics/btm404

Lee M, Rozeboom HJ, de Waal PP, de Jong RM, Dudek HM, Janssen DB (2017) Metal Dependence of the Xylose Isomerase from *Piromyces* sp. E2 Explored by Activity Profiling and Protein Crystallography. Biochemistry 56:5991–6005. https://doi.org/10.1021/acs.biochem.7b00777

Li Y, Zhu Y, Liu A, Sun Y (2011) Identification and characterization of a novel L-arabinose isomerase from *Anoxybacillus flavithermus* useful in D-tagatose production. Extremophiles 15:441–450. https://doi.org/10.1007/s00792-011-0375-2

Luo Y, Zhang T, Wu H (2014) The transport and mediation mechanisms of the common sugars in *Escherichia coli*. Biotechnol Adv 32:905–919. https://doi.org/10.1016/j.biotechadv.2014.04.009

Madhavan A et al (2009) Xylose isomerase from polycentric fungus *Orpinomyces*: gene sequencing, cloning, and expression in *Saccharomyces cerevisiae* for bioconversion of xylose to ethanol. Appl Microbiol Biotechnol 82:1067–1078. https://doi.org/10.1007/s00253-008-1794-6

Mathews II et al (2008) Crystal structure of 2-keto-3-deoxygluconate kinase (TM0067) from *Thermotoga maritima* at 2.05 Å resolution. Proteins 70:603–608

Neifar S et al (2019) A novel thermostable and efficient Class II glucose isomerase from the thermophilic *Caldicoprobacter algeriensis*: Biochemical characterization, molecular investigation, and application in High Fructose Syrup production. Int J Biol Macromol 129:31–40. https://doi.org/10.1016/j.ijbiomac.2019.01.150

Nunn CE, Johnsen U, Schönheit P, Fuhrer T, Sauer U, Hough DW, Danson MJ (2010) Metabolism of pentose sugars in the hyperthermophilic archaea *Sulfolobus solfataricus* and *Sulfolobus acidocaldarius*. J Biol Chem 285:33701–33709

O'Leary NA et al (2016) Reference sequence (RefSeq) database at NCBI: current status, taxonomic expansion, and functional annotation. Nucleic Acids Res 44:D733–745. https://doi.org/10.1093/nar/gkv1189

Park J, Gupta RS (2008) Adenosine kinase and ribokinase–the RK family of proteins. CMLS 65:2875–2896. https://doi.org/10.1007/s00018-008-8123-1

Patrick JW, Lee N (1969) Subunit structure of L-arabinose isomerase from *Escherichia coli*. J Biol Chem 244:4277–4283

Pickl A, Johnsen U, Archer RM, Schönheit P (2014) Identification and characterization of 2-keto-3-deoxygluconate kinase and 2-keto-3-deoxygalactonate kinase in the haloarchaeon *Haloferax volcanii*. FEMS Microbiol Lett 361:76–83

Pickl A, Johnsen U, Schönheit P (2012) Fructose degradation in the haloarchaeon *Haloferax volcanii* involves a bacterial type phosphoenolpyruvate-dependent phosphotransferase system, fructose-1-phosphate kinase, and class II fructose-1,6-bisphosphate aldolase. J Bacteriol 194:3088–3097

Prabhu P, Tiwari MK, Jeya M, Gunasekaran P, Kim IW, Lee JK (2008) Cloning and characterization of a novel L-arabinose isomerase from *Bacillus licheniformis*. Appl Microbiol Biotechnol 81:283–290. https://doi.org/10.1007/s00253-008-1652-6

Robert X, Gouet P (2014) Deciphering key features in protein structures with the new ENDscript server. Nucleic Acids Res 42:W320–W324

Son H, Lee SM, Kim KJ (2018) Crystal structure and biochemical characterization of xylose isomerase from *Piromyces* sp. E2. J Microbiol Biotechnol 28:571–578. https://doi.org/10.4014/jmb.1711.11026

Staudigl P, Haltrich D, Peterbauer CK (2014) L-Arabinose isomerase and D-xylose isomerase from *Lactobacillus reuteri*: characterization, coexpression in the food grade host *Lactobacillus plantarum*, and application in the conversion of D-galactose and D-glucose. J Agric Food Chem 62:1617–1624. https://doi.org/10.1021/jf404785m

Sutter JM, Johnsen U, Schönheit P (2017) Characterization of a pentonolactonase involved in D-xylose and L-arabinose catabolism in the haloarchaeon *Haloferax volcanii*. FEMS Microbiol Lett. https://doi.org/10.1093/femsle/fnx140

Umemoto Y, Shibata T, Araki T (2012) D-xylose isomerase from a marine bacterium, *Vibrio* sp. strain XY-214, and D-xylulose production from beta-1,3-xylan. Mar Biotechnol (NY) 14:10–20. https://doi.org/10.1007/s10126-011-9380-9

van de Werken HJ, Brouns SJ, Van der Oost J (2008) Pentose metabolism in archaea. In: Blum P (ed) Archaea. Caister Academic Press, New Models for Prokaryotic Biology, pp 71–94

Wagner M et al (2018) *Sulfolobus acidocaldarius* transports pentoses via a carbohydrate uptake transporter 2 (cut2)-type ABC transporter and metabolizes them through the aldolase-independent Weimberg Pathway. Appl Environ Microbiol. https://doi.org/10.1128/AEM.01273-17

Wanarska M, Kur J (2012) A method for the production of D-tagatose using a recombinant *Pichia pastoris* strain secreting beta-D-galactosidase from *Arthrobacter chlorophenolicus* and a recombinant L-arabinose isomerase from *Arthrobacter sp.* 22v. Microb Cell Fact 11:113. https://doi.org/10.1186/1475-2859-11-113

Wang H, Yang R, Hua X, Zhang Z, Zhao W, Zhang W (2011) Expression, enzymatic characterization, and high-level production of glucose isomerase from *Actinoplanes missouriensis* CICIM B0118(A) in *Escherichia coli* Zeitschrift fur Naturforschung C. J Biosci 66:605–613. https://doi.org/10.1515/znc-2011-11-1210